Translocation of Human Calcitonin in Respiratory Nasal Epithelium Is Associated with Self-Assembly in Lipid Membrane

Maria Christiane Schmidt, Barbara Rothen-Rutishauser, Beate Rist, Annette Beck-Sickinger, Heidi Wunderli-Allenspach, Werner Rubas,‡ Wolfgang Sadée,§ and Hans Peter Merkle*

Department of Pharmacy, Swiss Federal Institute of Technology Zurich (ETH), Irchel Campus, Winterthurerstrasse 190, CH-8057 Zurich, Switzerland, Genentech Inc., South San Francisco, California, Department of Biopharmaceutical Sciences and Pharmaceutical Chemistry, University of California, San Francisco, California

Received May 22, 1998; Revised Manuscript Received September 21, 1998

ABSTRACT: We studied the mechanisms involved in the translocation of human calcitonin (hCT) through excised bovine nasal mucosa (net mucosal-to-serosal permeability $\sim 10^{-5}$ cm s^{-1}). To determine structural requirements for the suggested vesicular internalization two carboxyfluorescein-labeled (fl) hCT fragments, the C-terminal fragment [N_α-fl]hCT(9−32) and the N-terminal fragment [Lys(fl)^{18}]hCT(1−24) were synthesized. In presence of the endocytosis inhibitor cytochalasin D mucosal-to-serosal and serosal-to-mucosal hCT permeabilities were equal. Pathway visualization by confocal laser scanning microscopy showed punctated fluorescence indicating vesicular internalization of both hCT and [N_α-fl]hCT(9−32). In contrast, the N-terminal fragment lacking the β-sheet forming C-terminus (25−32) was not internalized. Circular dichroism showed that, when interacting with neutral and negatively charged liposomes, hCT adopts β-sheet conformation. In a concentrated aqueous solution, β-sheet formation induces hCT self-assembly and fibrillation. High partitioning of hCT into lipid bilayer membranes was reflected by an apparent partition coefficient log D(pH 7.4) = 2.5 (liposome-buffer equilibrium dialysis). We propose that the high lipid partitioning and β-sheet formation result in C-terminus-restricted supramolecular self-assembly of hCT and [N_α-fl]hCT(9−32) in lipid membranes. Vesicular internalization is suggested to be associated with self-assembly induced perturbation of the lipid bilayer. Condensed hCT self-assemblies may explain the high capacity of net mucosal-to-serosal hCT permeation, which compares favorably with the low transport capacity of receptor-mediated endocytosis.

For most peptides, passage through biological membranes is compromised by low intrinsic membrane permeability and rapid clearance by membrane-associated proteolytic enzymes. Surprisingly, rather polar calcitonins, e.g., human, salmon, and eel calcitonin, can penetrate the nasal epithelium efficiently and are administered intranasally for therapeutic use. Human calcitonin (hCT),[1] a peptide hormone of 32 amino acids, is approved for the therapeutic treatment of established osteoporosis (*1*). Although plasma concentrations after nasal hCT administration remain low, the resulting hypocalcemic effect was similar to i.v. injection (*2*). There are only few other examples of successful transepithelial peptide drug delivery. For instance, (i) di- and tripeptides recognized by the common peptide transporters are efficiently taken up in the small intestine (*3*); (ii) the cyclic peptide cyclosporine A permeates through several membranes because of its high lipophilicity (*4*); and (iii) Rojas et al. (*5*) used a 12 amino acid residue membrane-translocating peptide sequence to engineer a glutathione *S*-transferase fusion protein and showed that this improved its import into cells. In contrast to these examples, membrane translocation of most therapeutic peptides is poor.

Mechanistic studies on hCT transport through excised bovine respiratory nasal mucosa have previosly demonstrated an unexpected nonsaturable net flux (net permeability $\sim 10^{-5}$ cm s^{-1}) in the mucosal-to-serosal direction (*6, 7*). Furthermore, punctated intracellular distribution of hCT indicated the involvement of endocytosis (*6*). Cremaschi et al. (*8*) proposed receptor-mediated endocytosis to explain the permeation of [1,7Asu]eel calcitonin through rabbit nasal mucosa.

The primary structure of hCT contains several domains relevant to its biological function. The N-terminal portion, cyclized by a disulfide bridge, is conserved between species and considered specific for receptor activation (*9*). In the central region, all calcitonins contain regularly spaced hydrophobic amino acids at every third or fourth residue, which is a typical feature of amphipathic α-helices that can bind to lipids (*10*). Finally, by spectroscopy the fibrillation of hCT solutions was observed to be associated with β-sheet formation in the C-terminal segment (*11, 12*).

Secondary structures of calcitonin have shown to be relevant for pharmacological activity as demonstrated by analogues with different α-helical contents (*13*). However, the potential of other, nonhelical conformations for hypo-

* Author to whom correspondence should be addressed, Department of Pharmacy. Phone: ++41 1 635 60 10. Fax: ++41 1 635 68 81. E-mail: Hmerkle@pharma.ethz.ch.

‡ Genentech Inc.

§ Department of Biopharmaceutical Sciences and Pharmaceutical Chemistry.

[1] Abbreviations: hCT, human calcitonin; CLSM, confocal laser scanning microscopy; PhC, phosphatidylcholine; log D, apparent partition coefficient; m-to-s, mucosal-to-serosal; s-to-m, serosal-to-mucosal; CD, circular dichroism spectroscopy.

10.1021/bi981219h CCC: $15.00
Published on Web 11/06/1998

calcemic activity is not clear (*13*). Epand et al. (*14*) demonstrated the formation of amphipathic helices in the presence of certain phospholipids, whereas interaction with lipid bilayers has yet to be studied. In aqueous solution, hCT has a tendency to form supramolecular self-assemblies in the form of fibrils, characterized by β-pleated sheet structures (*12*). Assemblies of hCT were found in amyloid fibrils present in granules of carcinoma of the thyroid (*15*). The pathological conversion of proteins to β-sheet containing toxic analogues has been shown, e.g., for the Alzheimer β-amyloid peptide (*16*) and for the infectious prion analogue PrPSc (*17*). The ability of hCT to self-assemble in membranes may be relevant to its physiological storage. Whether the structure responsible for biological activity is related to the proposed vesicular transport of hCT is unknown.

In the present study, we investigated the translocation of hCT in nasal mucosa. We demonstrate that hCT avidly associates with lipid membranes, assuming a conformation partially consisting of β-pleated sheets. Moreover, a C-terminal fragment of hCT, without the N-terminal loop critical for hypocalcemic activity (*9*), is also internalized, possibly via endocytosis. We assume that the ability of hCT to form supramolecular β-sheet assemblies in the lipid membrane plays an important role in a yet unknown endocytotic pathway.

MATERIALS AND METHODS

Chemicals. Sodium heptanesulfonic acid and tetramethylammonium hydroxide were obtained from Fluka (Buchs, Switzerland). Dulbecco's modified PBS (pH 7.2) consisted of (mM) NaCl (133.4); KCl (2.7); $MgCl_2 \cdot 6H_2O$ (0.5); $CaCl_2$ (1.2); KH_2PO_4 (1.15); $Na_2HPO_4 \cdot 2H_2O$ (8.1); D-glucose-(5.5). ^{3}H-mannitol (specific activity, 19.7 Ci/mmol) was from Du Pont de Nemours International SA (Le Grand-Saconnex, Switzerland). Egg phosphatidylcholin grade 1 was from Lipid Products (Nuttfield, Surrey, U.K.). Dipalmitoylphosphatidylglycerol and dipalmitoylphosphatidylcholine (DPPG/DPPC) were a gift from Sygena Ltd. (Liestal, Switzerland). Fmoc-protected amino acids and 4-(2',4'-dimethoxyphenyl-Fmoc-aminomethyl)-phenoxy resin were obtained from NovaBiochem (Läufelfingen, Switzerland), diisopropylcarbodiimide and thiocresol from Aldrich (Buchs, Switzerland), and 1-hydroxybenzotriazole, trifluoroacetic acid, thioanisole, diisopropylethylamine, piperidine, 4(5)-carboxyfluorescein, trifluoroethanol (TFE), and carboxyfluorescein isothiocyanate from Fluka. Dimethylformamide (p.a. grade), diethyl ether, acetonitrile and *tert*-butyl alcohol were purchased from Merck (Dietikon, Switzerland). All other chemicals used were of analytical grade.

Peptides. Human calcitonin (hCT) was kindly provided by Novartis Pharma AG (Basle, Switzerland). Two hCT fragments were synthesized. Peptide sequences were as follows:

hCT :

C G N L S T C M L G T Y T Q D F N K F H T F P Q T A I G V G A P-NH_2

[N_α-fl]hCT(9-32):

(fl)- L G T Y T Q D F N K F H T F P Q T A I G V G A P-NH_2

[Lys(fl)^{18}]hCT(1-24):

C G N L S T C M L G T Y T Q D F N K(fl)- F H T F P Q-NH_2

Synthesis of hCT Fragments, Labeling, and Identification. Linear hCT fragments were synthesized according to Rist et al. (*18*) by automated multiple solid-phase peptide synthesis using a robot system (Syro, MultiSynTech, Bochum, Germany).

HCT(9−32) was labeled at the N-terminus with 4(5)-carboxyfluorescein, while the peptide was still bound to the resin with fully protected side chains (*19*). Coupling was performed using a 3-fold excess of 4(5)-carboxyfluorescein, diisopropylcarbodiimide, and 1-hydroxy-benzotriazole. After 2 h, a 2-fold excess of diisopropylethylamine was added. The overall coupling time was 5 h.

For hCT(1−24), *tert*-butyloxy-carbonyl-Cys(trityl) [Boc-Cys(Trt)] was coupled at the N-terminus. Furthermore, the lysine in position 18 was side chain protected with 1-(4,4-dimethyl-2,6-dioxocyclohexylidene)ethyl (Dde). First, the resin was treated 5 times for 3 min with 2% hydrazine in dimethylformamide to remove the Dde group. Subsequently, Lys^{18} was labeled with a 5-fold excess of carboxyfluorescein isothiocyanate dissolved in dimethylformamide and a 3-fold excess of diisopropylethylamine. The linear fluorescence labeled peptide amides were cleaved with trifluoroacetic acid/thioanisole/thiocresol within 3 h, collected by centrifugation, and lyophilized from water. For air oxidation, the unprotected [Cys(SH)^{2,7}, Lys(fl)^{18}]hCT(1−24) was dissolved in 10 mM ammonium acetate buffer (pH 8.5) at a concentration of 1 mM. The solution was stirred for 24 h. The peptides were purified (>94%) by reversed-phase HPLC on a nucleosil C-18 column (Waters, Rupertswil, Switzerland) under isocratic conditions between 25 and 35% acetonitril.

Analysis of the peptides was performed on a nucleosil C-18 column: 5 μm, 3 × 125 mm (Merck AG). The mobile phases consisted of 0.1% (V/V) trifluoroacetic acid for A, and 100% acetonitrile for B. A gradient from 15 to 60% B in 30 min was used. The expected molecular weight was verified by ion-spray mass spectrometry (API III, Sciex, Toronto).

Peptide Quantification. The HPLC method described by Buck and Maxl (*20*) was applied. Mobile phases consisted of water:1 M tetramethylammonium hydroxide:acetonitrile, 88:2:10 (V/V) for A and 392:8:600 (V/V) for B. The pH was adjusted to 2.5 with phosphoric acid. A linear gradient from 30 to 50% B was applied. UV detection was set at 214 nm. Acetic acid (100 μL, 1 M) was added to 200 μL of sample solution to ensure peptide stability. Injection volume was 200 μL.

Excised Bovine Nasal Mucosa. Bovine nasal mucosa was obtained from freshly slaughtered cattle at the local slaughterhouse in Zurich (Schlachthaus AG, Switzerland) and prepared for the experiments as described by Lang et al. (*6, 21*). Briefly, excised tissue samples were inserted into the diffusion chambers, either the mucosal or the serosal side of the mucosa facing the donor compartment. Cell volume was 3 mL. For equilibration, the mucosae were preincubated with preheated PBS for 30 min.

Permeation Experiments Using Endocytosis Inhibitors. For permeation studies, commercially available Ussing chambers (Vertical diffusion chamber system, Corning Costar, Acton, MA) equipped with Ag−AgCl electrodes (Corning Costar) were used. The VCC MC6 Multi-Channel Clamp (Physiologic Instrument Inc., San Diego, CA) connected to a PC was used to control the transepithelial current.

Routinely, temperature was set at 37 °C and stirring was by a constant oxygen gas flow. After equilibration, buffer solution was replaced by 60 μM hCT solution on the donor and by pure PBS on the receiver side, respectively. To prevent hCT aggregation and ensure sufficient physical stability, 0.1% (m/V) hydroxypropylmethylcellulose (Methocel K4M; Prochem AG, Zurich, Switzerland) was added to the donor solution (*6*). Permeability of hCT in excised bovine nasal mucosa (*6*) was shown to be independent of concentration (1−60 μM). As endocytosis inhibitors, either colchicine (20 μM; Sigma, Buchs, Switzerland) or cytochalasin D (0.1 μg mL^{-1}; Fluka, Buchs, Switzerland) was added to both chambers. Samples of 0.2 mL were taken every 10 min up to 60 min from the receiver side and replaced by pure preheated buffer solution. After 30 and 50 min, samples of 0.05 mL were taken from the donor side.

Mucosal integrity was assessed using [^{3}H]mannitol at an initial concentration of 0.5 μCi mL^{-1}. Samples of 0.1 mL were taken from the receiver at 10, 40, and 50 min, added to 2 mL of scintillation cocktail (Ultima Gold, Packard, The Netherlands) and counted using a liquid scintillation spectrometer (Beckmann Instruments Inc., Fullerton, CA).

Effective permeability coefficients P_{eff} (cm s^{-1}) were calculated according to eq 1:

$$P_{\text{eff}} = \left(\frac{\mathrm{d}C}{\mathrm{d}t}\right)_{\text{ss}} \frac{V}{AC_{\text{D}}} \qquad (1)$$

$(\mathrm{d}C/\mathrm{d}t)_{\text{ss}}$ = pseudo steady-state change of concentration over time (mmol mL^{-1} s^{-1}), A (cm^2) = permeation area, and V (mL) = volume of the receiver compartment, C_{D} (mmol mL^{-1}) = initial concentration in the donor compartment.

Tissue Preparations for Confocal Laser Scanning Microscopy. After excision, tissue samples were preincubated on a membrane holder with PBS for 10 min at 37 °C. For incubations at low temperature, mucosae were equilibrated at 4 °C prior to peptide incubation. After equilibration, the buffer solution was removed, and 0.1 mL of peptide solution was added. Peptide concentrations were between 10 and 15 μM for the fluorophore-labeled peptide fragments, and 10 and 30 μM for hCT. After 10 min incubation, tissues were washed five times with 0.1 mL of PBS. For antibody staining, the tissues were fixed with *p*-formaldehyde [3% in PBS, [N_α-fl]hCT(9−32) in Figure 2i] for 1 h or acetone (for hCT, Figure 2a-e) for 20 min at room temperature and permeabilized with Triton X-100 (0.2% in PBS) for 1 h. PFA was not a suitable fixativum for hCT antibody staining in nasal tissue.

For hCT localization, tissues were washed, fixed with acetone as described above, and incubated with anti-rabbit polyclonal antibody to hCT (1:20, Anawa Trading SA, Wangen, Switzerland). Routinely, incubation times were 1 h at 37 °C plus 6 h at 4 °C. In addition, some tissue samples were incubated with anti-transferrin receptor (CD71) monoclonal antibody (1:50, Anawa). For coincubations of [N_α-fl]hCT(9−32) and hCT, a monoclonal antibody to residues 1−10 of hCT was used (anti-mouse, 1:20, Anawa) to avoid binding of the antibody to the fragment. After five washing steps, tissues were incubated with a fluorescence labeled secondary antibody (indodicarbocyamine Cy2, Cy3, or Cy5, 1:50, Juro Supply AG, Lucerne, Switzerland). Incubation times were as before. Additionally, nuclei were stained with 4,6-diamidino-2-phenylindole (DAPI, Hoechst Marion Roussel AG, Zurich, Switzerland) and tight junctions with anti rat ZO-1 (1:20, Juro Supply). Finally, tissues were mounted in Moviol (Juro Supply AG).

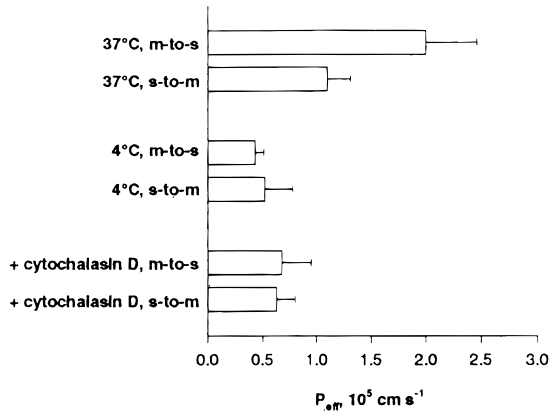

FIGURE 1: Influence of endocytosis inhibitor on the permeability of human calcitonin through excised bovine nasal mucosa. Initial hCT donor concentration was 60 μM. Permeability m-to-s versus s-to-m (*6*) was significantly different (*t*-test, $p < 0.05$). Cytochalasin D reduced significantly the m-to-s (*t*-test; $p < 0.001$, compared to m-to-s without inhibitor at 37 °C) and the s-to-m flux (t-test; $p < 0.01$, compared to s-to-m without inhibitor at 37 °C). Values at 37 and 4 °C were adapted from Lang et al. (*6*). Values are expressed as the means ± SD of 5−7 determinations.

Nasal tissues fixed with PFA were also stained with rhodamine-phalloidin to label actin (Juro Supply AG). Some images were taken of unfixed tissue and incubated with the fluorophore labeled fragments for 10 min at 37 °C.

Visualization by Confocal Laser Scanning Microscopy (CLSM). A Zeiss LSM 410 inverted microscope (Zeiss AG, Zurich, Switzerland) was used with the following lasers: HeNe 633 nm, HeNe 543 nm, Ar 488/514 nm, and Ar UV 364 nm. Optical sections at intervals of 0.25 μm were taken with a 63×/1.4 Plan-Apochromat objective. Image processing was done on a Silicon Graphics workstation using IMARIS, a 3D multichannel image processing software for confocal microscopic images (Bitplane AG, Zurich, Switzerland). The processed data sets were illustrated as single layers or as projections ($x-z$ and $y-z$) by cutting sections orthogonally to the recording plane ($x-y$). The degree to which two labels in a sample are distributed identically was analyzed using the colocalization software (Bitplane AG, Zurich, Switzerland).

Liposomes for Partition Experiments. Unilamellar egg phosphatidylcholine (PhC) liposomes were prepared using the extrusion method as described by Ottiger and Wunderli (*22*). The lipid concentration was determined with a phospholipase D-choline oxidase-peroxidase assay for PhC (MPR 2, Boehringer-Mannheim, Mannheim, Germany). The size distribution was measured by dynamic light scattering on a Nicomp 370 (Particle Sizing Systems, Santa Barbara, CA).

Partition Experiments. Liposome-buffer partition experiments were performed by equilibirum dialysis as described by Pauletti et al. (*23*). Macro 1 dialysis cells (Dianorm, Munich, Germany) equipped with cellulose dialysis membranes (Diachema, MW cut-off 10 000, Dianorm) were mounted within the Dianorm-4 drive cell carrier. Chambers were filled with 1 mL of PhC liposome suspension (4 mM

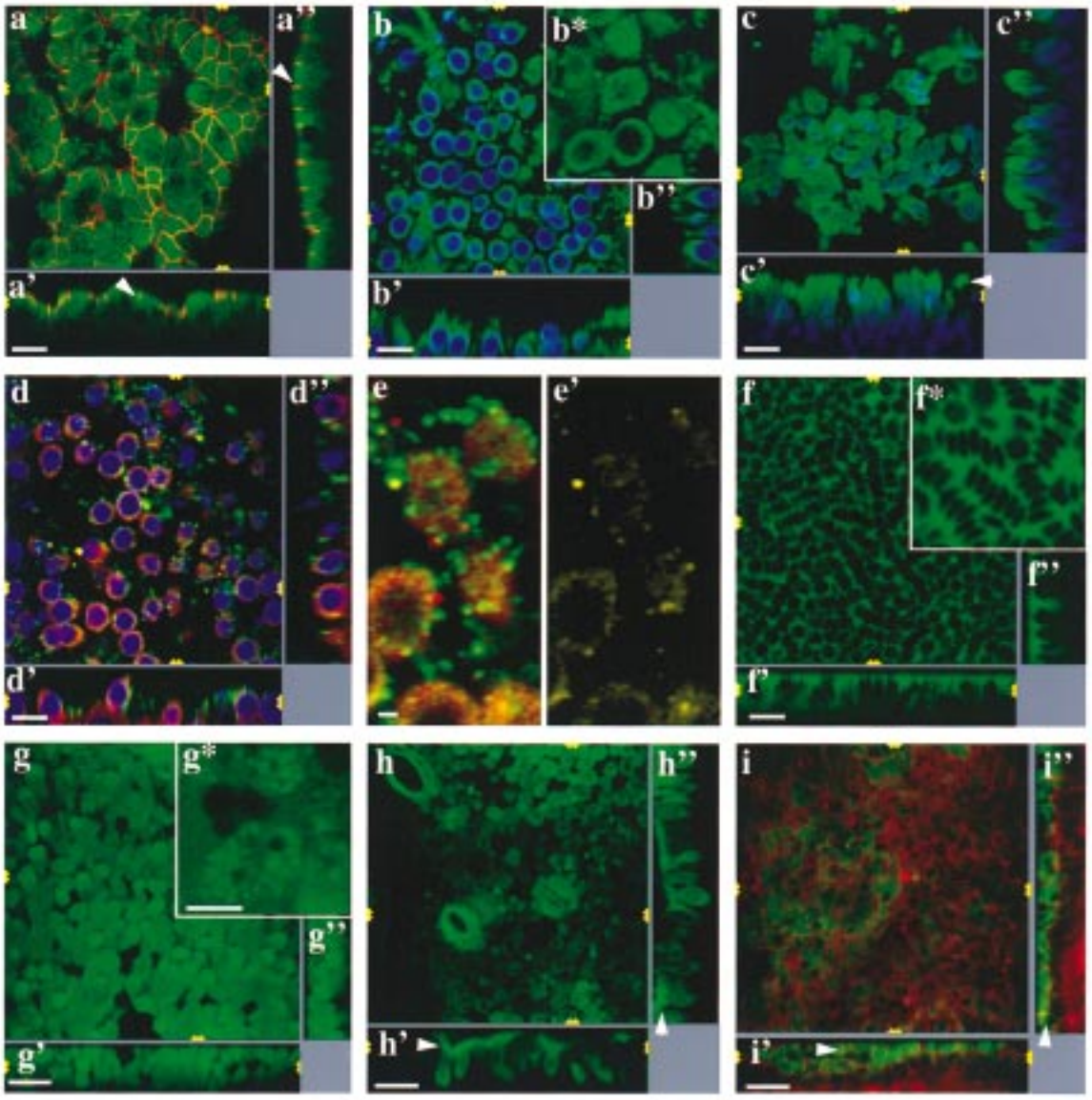

FIGURE 2: Visualization of transport pathways of hCT and two hCT fragments in nasal epithelium by CLSM. Peptides are shown in green. ZO-1 (a), transferrin receptor (d, e), and F-actin (i) are shown in red. The cell nuclei (b, c, d) are shown in blue. Analyzed colocalization of the transferrin receptor and hCT is shown in yellow (e′). After hCT permeation under various conditions the nasal epithelium has been fixed and stained with antibodies or fluorescence labeled markers (a−e, i), whereas optical sections shown in panels f−h have been taken in unfixed tissue. hCT is highly concentrated in the membrane and intracellular space, the arrowheads point to tight junctions which are localized near the apical surface (a). At lower concentration, hCT shows a punctated pattern (b). Internalization of hCT was blocked at reduced temperature, the arrowhead indicates the mucosa surface (c). Double-labeling of the transferrin receptor and hCT indicates colocalization of the two proteins (d, e), which was analyzed and is shown in e′. The N-terminal fragment was not internalized into the cell (f), in contrary to the C-terminal fragment (g). A punctated fluorescence of the C-terminal fragment can clearly be shown at higher magnification (g*). Internalization was markedly reduced in the presence of cytochalasin D (h) as well as at 4 °C (i). The peptide remaining on the mucosal surface is shown by arrowheads. Pictures a, b, c, d, f, g, h, and i represent *xy*-projections from all the layers between the two yellow arrowheads shown in the xz-picture; pictures a′, b′, c′, d′, *f* ′, g′, h′, and i′ represent *xz*-projections from all the layers between the two yellow arrowheads shown in the xy-picture; and pictures a″, b″, c″, d″, *f* ″ g″, h″, and i″ represent *yz*-projections from all the layers between the two yellow arrowheads shown in the *xy*-picture. Scale bars: a, b, c, d, f, 10 μm; e, e′, 2 μm; g, h, i, 20 μm; b*, f*, g*, 10 μm.

PhC in PBS pH 7.4) containing 10 μM hCT on one and PBS on the other side. Incubation times were 15, 30, 45 min, 1, 2, 3, 5, and 7 h in order to determine the equilibrium. The stability of the PhC liposomes over this time range at 37 °C has been reported by Ottiger et al. (*22*). Temperature was at 37 °C. For HPLC analysis, liposomes were dissolved in methanol (1:3, v/v). The recovery rate was 96.8 ± 4.8%. The values at 7 h were used for calculation of the apparent partition coefficient.

The apparent partition coefficient (D) was calculated according to:

$$D = \frac{V_L(c_L - c_B)}{V_{Lipo}c_B} + 1 \qquad (2)$$

where $V_{Lipo} = nN_AV_M$. V_L is the sample volume (m^3), c_L and c_B are the peptide concentrations (mol L^{-1}) on the buffer (c_B), respectively. On the liposome (c_L) side in the dialysis

equilibrium, n is the number of moles of lipid in V_L, N_A is Avogadro's number (6.022×10^{23} mol^{-1}), and V_M is the volume per lipid molecule in the bilayer [1.253×10^{-27} m^3 for PhC (*24*)].

Circular Dichroism Spectroscopy (CD). CD measurements were carried out on a Jasco J720A spectropolarimeter (Jasco, Tokyo, Japan) with a wavelength range from 240 to 180 nm in a nitrogen atmosphere. The quartz sample cell had a path length of 0.1 cm, the scan speed was 20 nm min^{-1}, and the response time was 4 s. A minimum of three spectra was accumulated for each sample. Peptide concentrations were 100 μM, except for the pure PBS solution, where the hCT concentration was reduced to 10 μM because of the low solubility and fibrillation of hCT in this medium. In liposomal suspensions, up to 100 μM hCT was soluble. Studies were performed in PBS and in the "membrane-mimicking" media trifluoroethanol (TFE, 100%) and SDS micelles (100 mM SDS in 5 mM phosphate buffer, pH 7.4) at 21 °C. For membrane-binding studies, hCT was added to PhC lipsomes (2 mM in PBS, prepared as described under liposomes for partition experiments). Additionally, negatively charged DPPG/DPPC liposomes (75:25 mol:mol) were prepared by sonication as described by Lee et al. (*25*) and diluted with PBS to a final concentration of 2 mM. Measurements were started after 10 min of equilibration at 37 °C. No visible hCT aggregates were observed in solution. The CD spectra are given as mean ellipticity Θ (deg cm^2 mol^{-1}). For calculation of the secondary structure elements the method of Yang et al. (*26*) has been applied, modified for peptides by replacing the reference sets as described by Behrends (*27*).

RESULTS

Permeation Studies. In a previous study, Lang et al. (*6*) showed the directional specificity of the transport of hCT using excised bovine nasal mucosa. Whereas at 37 °C, the mucosal-to-serosal (m-to-s) permeability was approximately 2-fold above the serosal-to-mucosal (s-to-m) permeability, directional specificity was abolished at 4 °C (Figure 1). The involved mechanism was investigated in the present study.

To determine whether the transport involves an endocytotic mechanism, permeation studies were also performed in the presence of two endocytosis inhibitors, cytochalasin D and colchicine. Cytochalasin D disrupts intracellular microfilaments that attach at or near the cell surface. The presence of 0.1 μg/mL^{-1} *cytochalasin D* reduced significantly ($p < 0.001$) the m-to-s flux of hCT as well as the flux in the s-to-m direction ($p < 0.01$) (Figure 1). The presence of cytochalasin D had no adverse effect on the integrity of the epithelium as judged from unchanged [^{3}H]mannitol flux P_{eff} [$(0.8 \pm 0.2) \times 10^{-4}$ cm s^{-2}, both directions] and constant transepithelial electrical resistance R_m ($\sim$30 Ω cm^2).

Permeabilities in the presence of 20 μM *colchicine* [m-to-s $(1.3 \pm 0.8) \times 10^{-5}$ cm s^{-2}; s-to-m $(1.3 \pm 0.7) \times 10^{-5}$ cm s^{-2}], which disrupts sorting, were too variable to permit evaluation of a significant effect on the flux of hCT. The permeabilities of [^{3}H]mannitol after colchicine treatment were increased by about 20% [m-to-s $(1.0 \pm 0.2) \times 10^{-4}$ cm s^{-2}; s-to-m $(1.0 \pm 0.3) \times 10^{-4}$ cm s^{-2}]. This may indicate that colchicine affected the integrity of the tight junctions, which would enhance the paracellular transport of hCT. In contrast, Cremaschi et al. (*28*) reported that colchicine did not affect junctional permeability of [1,7Asu]eel calcitonin in rabbit nasal mucosa. Due to this inconsistency colchicine data were excluded from further considerations.

CLSM Imaging. Previous CLSM studies revealed a vesicular-type distribution of fluorophore-labeled hCT, indicating endocytotic uptake of hCT in the nasal epithelium (*6*). Additional permeation and metabolism studies demonstrated that the fluorophore label did not affect peptide flux and metabolic rate (*6*). In the present study, we used antibody staining to detect the pathway of unlabeled hCT in the nasal epithelium. At high concentrations (30 μM), hCT accumulated at the surface of the mucosal membrane and in the cells but not in the paracellular space (Figure 2a). In further studies, hCT concentration was reduced to 10 μM in order to lower the fluorescence intensity on the mucosal surface caused by high hCT concentrations and to permit better detection of intracellularly located peptide. After a 10 min incubation, not only at the mucosal cell surface, but also in deeper sections, hCT showed a punctated pattern (Figure 2b*). The punctated fluorescence seemed to be concentrated around the nuclei which can be the result of shrinking caused by acetone fixation. Nuclei were localized in different depths within the epithelium (Figure 2b′) causing unequal appearance in the vertical section. Absence of peptide in the paracellular space may result from the washing, fixation, and permeabilization steps before antibody labeling.

The transferrin receptor, used to trace intracellular routing of clathrin-coated vesicles, cycles constitutively in the presence or absence of bound transferrin (*29*). The transferrin receptor is internalized into clathrin-coated pits, which become clathrin-coated vesicles. After losing their coats, the vesicles fuse with other vesicles or an existing endosome (*30*). To further characterize the endocytotic mechanism, we investigated whether hCT and the transferrin receptor are colocalized in the same vesicle-like structures. Figure 2d shows intensive staining of the transferrin receptors close to the serosal side, whereas no staining was observed close to the mucosal side. After 10 min of hCT incubation on the mucosal side, punctated hCT fluorescence appeared throughout the cell, although less frequently at the serosal side (Figure 2d). In some sections, hCT was colocalized with transferrin vesicles as indicated by the yellow fluorescence (Figure 2e). This was substantiated by a colocalization analysis with the IMARIS software (Figure 2e′). At 4 °C, internalization was inhibited and the presence of hCT was restricted to the mucosal surface (Figure 2c).

To further investigate the structural domains of hCT responsible for internalization, the cellular pathways of two fluorescence-labeled hCT fragments with C- and N-terminal truncations of 8 amino acid residues each were visualized by CLSM in unfixed tissue. The N-terminal fragment *[Lys-(fl)^{18}]hCT(1−24)* was exclusively associated with the membrane but not at all internalized into the cells (Figure 2f).

Application of the C-terminal fragment *[N$_\alpha$-fl]hCT(9−32)* to the mucosal side showed internalization in the form of punctated fluorescence (Figure 2, panels g and g*), indicating vesicular transport. The more diffuse fluorescence as compared to hCT (Figure 2b) can be explained by the higher susceptibility of [N$_\alpha$-fl]hCT(9−32) to intracellular metabolism and diffusion of the metabolites out of the vesicles. Indeed, in contrast to the more stable hCT (*21*), HPLC

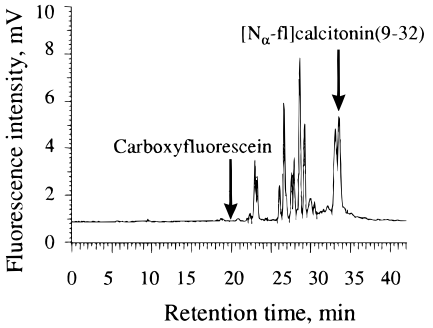

FIGURE 3: HPLC chromatogram of [N_α-fl]hct(9−32) (approximately 1 μM, RT 33.1 and 33.6 min) after exposure to bovine nasal mucosa for 15 min at 37 °C. Detection by fluorescence showed the appearance of fluorescence labeled metabolites. The fluorescence label was not released (RT of the carboxyfluorescein was determined at 19.8 min). Double-peak of [N_α-fl]hct(9−32) is explained by carboxyfluorescein isomers used for labeling. HPLC runs without peptide injection shows straight baseline at 1 mV.

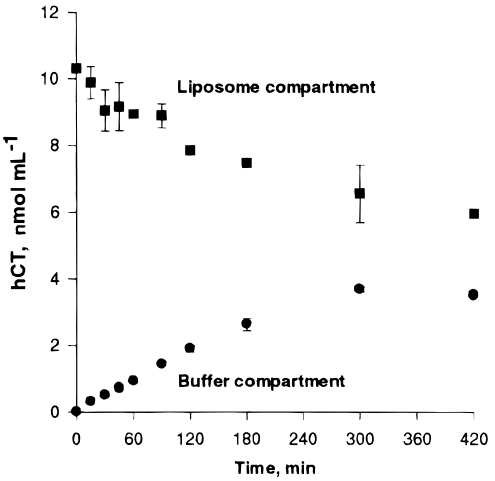

FIGURE 4: Partitioning of hCT 10 μM hCT in a phosphatidylcholine liposome-buffer equilibrium dialysis system. HCT concentrations in both compartements vs time. Equilibrium reached within 5 h as indicated by the plateau ($n = 3$, means ± SD, bars partly within the points).

analysis of incubated [N_α-fl]hCT(9−32) showed extensive metabolism to smaller fragments, without release of the fluorescent label (Figure 3). Internalization of [N_α-fl]hCT-(9−32) was not blocked by a 100-fold excess of coadministered hCT (data not shown). We also observed colocalization of the immunofluorescence of hCT and the concomitant autofluorescence of [N_α-fl]hCT(9−32). Further evidence for vesicular transport was obtained by incubation at 4 °C showing fluorescence at the mucosal surface (Figure 2i). Moreover, addition of 0.1 μg mL^{-1} cytochalasin D caused a drastic reduction of intracellular fluorescence, which suggests absence of vesicular transport (Figure 2h). In conclusion, truncation of the C-terminal portion of hCT blocked internalization into the cells, whereas the confocal images support the hypothesis of vesicular internalization of the C-terminal fragment.

Partition Experiments in Liposomes. To test the propensity of hCT to enter the cell membrane, partition coefficients were determined in a liposome-buffer equilibrium system (*23*). Unilamellar PhC liposomes were prepared by extrusion and had a diameter of 67 ± 6 nm. The partition coefficient (*D*) of hCT obtained by equilibrium dialysis was determined as log *D*(pH 7.4) = 2.5 ± 0.1 (values at 7 h, mean ± SD, $n = 3$). The equilibrium concentration at 7 h of hCT in the bilayer membrane was calculated as 0.8 mM compared to 3.5 μM in PBS (Figure 4). To the authors' knowledge, only log *D* values for the highly lipophilic cyclosporine A are available [log *D*(pH 7) ≈ 4, (*22*)]. In general, lipophilic compounds are characterized by a log *D* above 2. This documents a surprisingly high affinity of the relatively polar hCT toward lipid membranes.

CD Spectroscopy. Freshly prepared monomeric hCT solutions show little ordered secondary structure in PBS (Figure 5 (*11*)]. When fibrillating as a function of time and concentration, hCT assumes approximately 25% α-helical structure [300 μM hCT after 21 min. (*11*)]. Further studies, using attenuated total reflection Fourier transform infrared (ATR-FTIR) spectroscopy, indicated that, upon fibrillation, initially α-helical and β-sheet structures (∼10%) were equally prevalent, followed by significant β-sheet formation (∼25%) after 2 up to ∼40 h (*12*).

In this study, circular dichroism was used to assess secondary structure conformation of hCT in "membrane mimicking" media, such as TFE and SDS micelles, and in the presence of uncharged and charged liposomes. In TFE and in SDS micelles, hCT adopted α-helical conformation with a maximum at 196 nm and two minima at 205 and 222 nm (40 and 28% α-helix, respectively) (Figure 5). Turbidity of the liposome solution reduced the received signal but still permitted analysis of secondary structures. Neutral PhC liposomes strongly induced the formation of β-sheets, as indicated by the single negative minimum at 219 nm (57%, Figure 5). Because no negative minimum at 205−210 nm combined with a second negative minimum at 222 nm was found, we conclude that there are no α-helical structures. The same was found, but to a lesser extent, in the presence of negatively charged DPPC/DPPG liposomes (25% β-sheet, Figure 5). Hence, β-sheet formation appeared to be independent of lipid membrane charge. The lower content of β-sheet structures in the DPPC/DPPG vesicles (sonication; diameter 25 ± 13 nm) may be due to the less tightly packed lipids in these liposomes compared to the packing in larger PhC liposomes (extrusion; diameter 67 ± 6 nm). Liposome suspensions containing 100 μM hCT were stable for about 2−3 h, while higher peptide concentrations rapidly induced visible loss of liposomal organization.

DISCUSSION

So far, the mechanisms involved in the transport of hCT through nasal mucosa were largely unkown. Previously, a receptor-mediated uptake was postulated for [1,7Asu]eel calcitonin (*8*) but has not yet been confirmed (*28, 31*). In this work, we suggest that internalization of hCT into the mucosa is associated with β-sheet-induced self-assembly of the C-terminal segment of the peptide. In contrast, the helical content and the N-terminal segment are known to be important for CT receptor binding and biological activity (*32, 33, 34*).

The amino acid sequence of calcitonins undergoes considerable species variation but maintains a typical pattern in the C-terminal region (Figure 6). A highly conserved C-terminal motif is TXPXTXXGXGXP (human, eel, salmon, goldfish, etc.). This motif containing alternating small

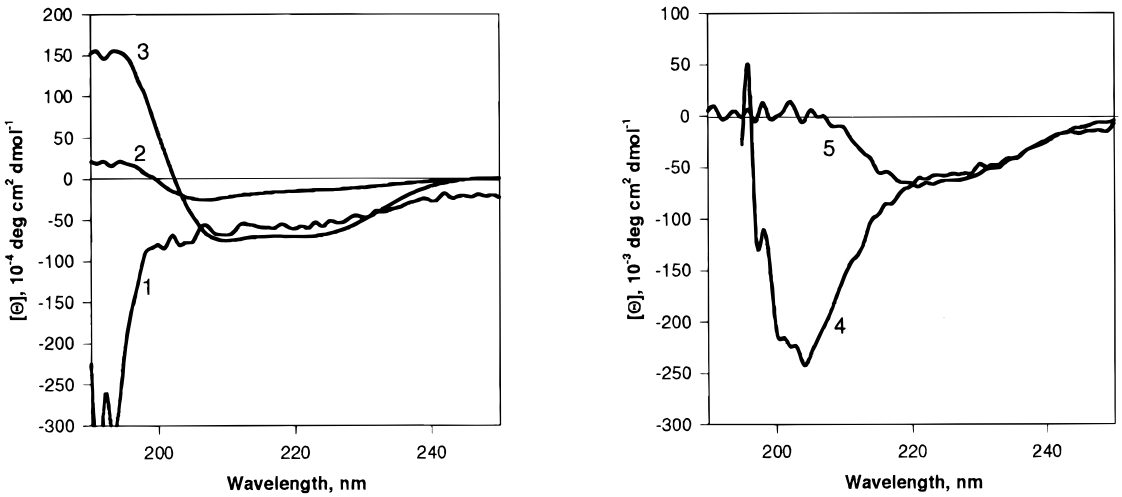

FIGURE 5: Effect of different media on the secondary structure of hCT monitored by CD. Conformation contents are given as percentages by H = α-helix, B = β-sheet, T = turn, R = random. Compared to the little ordered secondary structure in PBS (1, B 4%, R 96%), membrane mimicking media and phospholipids induced the formation of α-helices and/or β-sheets. Whereas in SDS micelles (2, H 28%, R 72%) and TFE (3, H 40%, B 40%, T 1%, R 19%) helical structures were preferred, hCT clearly formed a higher amount of β-sheet conformation in the presence of DPPC/DPPG (4, H 1%, B 25%, R 74%) and PhC liposomes (5, H 1%, B 57%, T 1%, R 41%). Peptide concentrations were 10 μM in PBS and 100 μM otherwise. Results are expressed as mean ellipticity, [Θ] (deg cm^2 dmol^{-1}).

```
 1 CSNLST CVLSAYWKDLNNYHR YSGMGFGPETP  32 (Ovis aries)
 2 CSNLST CVLSAYWKDLNNYHR FSGMGFGPETP  32 (Bovine)
 3 CSNLST CVLGTYSKDLNNFHT FSGIGFGAETP  32 (Canis familiaris)
 4 CSNLST CVLGKLSQDLHKLQT FPRTNTGAGVP  32 (Pink salmon)

 5 CSNLST CALGKLSQELHKLQS YPRTNVGAGTP  32 (Spotlined sardines)
 6 CSSLST CVLGKLSQELHKLQT YPRTNVGAGTP  32 (Goldfish)
 7 CSNLST CVLGKLSQELHKLQT YPRTDVGAGTP  32 (Japanese eel)
 8 CASLST CVLGKLSQELHKLQT YPRTDVGAGTP  32 (Gallus gallus)

 9 CASLST CVLGKLSQELHKLQT YPRTDVGAGTP  47 (Gallus gallus precursor)
10 CGNLST CMLGTYTQDFNKFHT FPQTAIGVGAP  32 (Human calcitonin)
11 CGNLST CILGTYTQDFNKFHT FPQTAIGVGAP 125 (Homo sapiens)
12 CGNLST CILGTYTQDFNKFHT FPQTAIGVGAP 141 (Homo sapiens preprocalcitonin)
```

FIGURE 6: Multiple sequence alignment of calcitonins. The numbers following the sequences indicate the length of the CT. For 9 (gallus gallus precursor), residues 12−43, for 11 (*Homo sapiens*), residues 69−100, and for 12 (*Homo sapiens* preprocalcitonin), residues 85−116 were used for the alignment. Besides the highly conserved N-terminus, responsible for CT receptor affinity, the β-sheet-type motif in the C-terminus (shaded), TXPXTXXGXGXP-amid, is conserved.

residues (T^{21}, T^{25}, G^{28}, G^{30}) and proline may mediate self-assembly via β-sheet formation. Another subset of calcitonins (ovine, bovine, and canine) contains an alternative motif: GXGXGXXXP. Analysis of the conformation of salmon calcitonin (sCT) fragments revealed that the biologically active sCT(1−23) assumes a helical structure upon interaction with dimyristoylphosphatidylglycerol, whereas the helical content of the biologically inactive sCT(12−32) was low (*33*). Since hCT(1−24) is not internalized by the nasal epithelium, it appears that helicity either plays no role or is not a sufficient prerequisite to internalize hCT into nasal epithelium. On the other hand, α-helical structure may account for the interaction of hCT(1−24) with the surface of the nasal membrane, as suggested by the remaining fluorescence on the cell surface even after several washing steps (Figure 2f). In contrast, in charged as well as in uncharged liposomes, hCT rapidly adopted β-sheet structures, which is analogous to the previously observed fibrillation of hCT in concentrated aqueous solutions (*11*, *12*). This suggests hypothetically that hCT assembles in the membrane independent of lipid charge to form condensed self-assemblies driven by β-sheet formation. Although liposomal dispersions do not permit direct extrapolation to the cellular level, they are considered to bear relevance, and represent a meaningful approach in the context of biological membranes. Previously, Arvinte and Drake (*35*) investigated the α-helicity of hCT in TFE−water mixtures. Helicity was found to develop above 11 mol % TFE and was assigned to amino acid positions 9−22. In pure TFE, 57% α-helix was observed.

The high partition coefficient in the liposome-buffer equilibrium system and the high solubility of hCT in liposomal suspensions can explain the high peptide concentrations in the membrane estimated to reach nearly 1 mM in our study. At such a concentration, hCT fibrillation in aqueous solution would be rapid. In contrast, Terzi et al. (*36*) showed for Alzheimer β-amyloid peptide that only

negatively charged vesicles induced a shift toward β-sheet structure formation leading to toxic fibril aggregation. Neutral vesicles had no effect. Furthermore, a decrease of negative membrane charges prevented membrane association of β-amyloid fibrils, showing that the association of the Alzheimer β-amyloid peptide may depend on electrostatic interactions with membrane lipids (*16*).

The directional specificity and the temperature sensitivity of the hCT flux supports the postulate of an active transport component through bovine nasal mucosa (*6*) (Figure 1). In addition, cytochalasin D reduced the m-to-s flux to the level of the s-to-m flux, indicating that active transcellular transport was inhibited. In contrast, in the presence of cytochalasin D, Cremaschi et al. (*31*) reported an increase of the s-to-m flux of [1,7Asu]eel calcitonin relative to the value of the m-to-s flux in rabbit nasal mucosa, indicating a higher fraction of paracellular diffusion. However, no membrane integrity marker, e.g., [^{3}H]mannitol, was used in their work as a control to confirm this hypothesis. As a first indication to explain the directional specificity of hCT transport, we observed (occasional) fusion of hCT containing vesicle-type structures with those containing the transferrin receptor. Since in nasal mucosa this receptor preferentially recycles at the serosal side, fusion of hCT and transferrin containing vesicles could account for the exocytosis on the serosal side and the positive net-flux of hCT.

C- and N-terminally truncated hCT fragments were used to determine the structural requirements for membrane uptake and vesicular internalization. Whereas, for the hydrophobic C-terminal fragment, endocytosis was observed, the more hydrophilic N-terminal fragment was not internalized. Therefore, intermolecular β-sheet formation based on the tail residues 23−32 (*11*, *12*) is proposed to lead to condensed self-assemblies for both intact hCT and the C-terminal fragment [N_α-fl]hCT(9−32) in the lipid membrane of the nasal mucosa. In contrast, [Lys(fl)^{18}]hCT(1−24) appears to lack the ability to form condensed self-assemblies in the mucosa for internalization. If hCT and the C-terminal fragment form β-sheets within the membrane, they could be embedded deeply into the lipid bilayer. This membrane integration could by itself produce the signal for vesicular internalization, for example, by bilayer perturbation. Indeed, CD (at 222 nm) and electron microscopy studies by Epand et al. (*14*) showed that human calcitonin is able to deform and solubilize multilamellar phosphatidylglycerol vesicles. Perturbation of lipid bilayers by pore-forming peptides was previously shown by Fattal et al. (*37*). Our results with [Lys(fl)^{18}]hCT(1−24) suggest that the formation of an amphipathic helix alone could not elicit such effects.

In conclusion, we propose that the transport of hCT into and across the nasal mucosal epithelium involves a yet unknown endocytotic mechanism. It appears that the suggested vesicular internalization of hCT and possibly of functionally conserved fragments is associated with C-terminus restricted self-assembly in the lipid membrane to form condensed β-sheet structures of yet unknown size, shape, and structure. The N-terminal domain of the peptide critical for its biological function is unrelated to this process. The condensed state provides the basis for high transport capacity by endocytosis and transcytosis of hCT in contrast to receptor-mediated endocytosis with its typical low throughput (*38*).

ACKNOWLEDGMENT

We gratefully acknowledge the following contributions: Dr. Cornelia Ottiker for instructions on liposome equilibrium dialysis, Maja Günthert for running the confocal microscope, Kati Zlinszky (Veterinary Pathology, University of Zurich) for optimizing the tissue fixation procedure for antibody staining, and Dr. Tudor Arvinte (Novartis Pharma AG, Basle) for discussions on the secondary structure of hCT.

REFERENCES

1. Silverman, S. L. (1997) *Am. J. Med. Sci. 313*, 13−16.
2. Pontiroli, A. E., Alberetto, M., and Pozza, G. (1985) *Br. Med. J. (Clin. Res. Ed.) 290*, 1390−1391.
3. Walter, E., Kissel, T., and Amidon, G. L. (1996) *Adv. Drug Deliv. Rev. 20*, 33−58.
4. Augustijns, P. F., Bradshaw, T. P., Gan, L. S., Hendren, R. W., and Thakker, D. R. (1993) *Biochem. Biophys. Res. Commun. 197*, 360−365.
5. Rojas, M., Donahue, J. P., Tan, Z., and Lin, Y.-Z. (1998) *Nat. Biotechnol. 16*, 370−375.
6. Lang, S., Rothen-Rutishauser, B., Perriard, J.-C., Schmidt, M. C., and Merkle, H. P. (1998) *Peptides 19*, 599−607.
7. Schmidt, M. C., Peter, H., Lang, S. R., Ditzinger, G., and Merkle, H. P. (1998) *Adv. Drug Deliv. Rev. 29*, 51−79.
8. Cremaschi, D., Rossetti, C., Draghetti, M. T., Manzoni, C., and Aliverti, V. (1991) *Pflüg. Arch. 419*, 425−432.
9. Stroop, S. D., Nakamuta, H., Kuestner, R. E., Moore, E. E., and Epand, R. M. (1996) *Endocrinology 137*, 4752−4756.
10. Epand, R. M., Epand, R. F., Orlowski, R. C., Seyler, J. K., and Colescott, R. L. (1986) *Biochemistry 25*, 1964−1968.
11. Arvinte, T., Cudd, A., and Drake, A. F. (1993) *J. Biol. Chem. 268*, 6415−6422.
12. Bauer, H. H., Muller, M., Goette, J., Merkle, H. P., and Fringeli, U. P. (1994) *Biochemistry 33*, 12276−12282.
13. Kapurniotu, A., and Taylor, J. W. (1995) *J. Med. Chem. 38*, 836−847.
14. Epand, R. M., Epand, R. F., Orlowski, R. C., Schlueter, R. J., Boni, L. T., and Hui, S. W. (1983) *Biochemistry 22*, 5074−5084.
15. Silver, M. M., Hearn, S. A., Lines, L. D., and Troster, M. (1988) *J. Histochem. Cytochem. 36*, 1031−1036.
16. Hertel, C., Terzi, E., Hauser, N., Jakob-Rotne, R., Seelig, J., and Kemp, J. A. (1997) *Proc. Natl. Acad. Sci. U.S.A. 94*, 9412−9416.
17. Baldwin, M. A., Pan, K. M., Nguyen, J., Huang, Z., Groth, D., Serban, A., Gasset, M., Mehlhorn, I., Fletterick, R. J., and Cohen, F. E. (1994) *Philos. Trans. R. Soc. London B, Biol. Sci. 343*, 435−441.
18. Rist, B., Enzeroth, M., and Beck-Sickinger, A. G. (1998) *J. Med. Chem. 41*, 117−123.
19. Weber, P. J. A., Bader, J. E., Folkers, G., and Beck-Sickinger, A. G. (1998) *Bioorg. Med. Chem. Lett. 8*, 597−600.
20. Buck, R. H., and Maxl, F. (1990) *J. Pharm. Biomed. Anal. 8*, 761−769.
21. Lang, S. R., Staudenmann, W., James, P., Manz, H. J., Kessler, R., Galli, B., Moser, H. P., Rummelt, A., and Merkle, H. P. (1996) *Pharm. Res. 13*, 1679−1685.
22. Ottiger, C., and Wunderli-Allenspach, H. (1997) *Eur. J. Pharm. Sci. 5*, 223−231.
23. Pauletti, G. M., and Wunderli-Allenspach, H. (1994) *Eur. J. Pharm. Sci. 1*, 273−282.
24. Huang, C., and Mason, J. T. (1978) *Proc. Natl. Acad. Sci. U.S.A. 75*, 308−310.
25. Lee, S., Yoshitomi, H., Morikawa, M., Ando, S., Takiguchi, H., Inoue, T., and Sugihara, G. (1995) *Biopolymers 36*, 391−398.
26. Yang, J. T., Wu, C. S., and Martinez, H. M. (1986) *Methods Enzymol. 130*, 208−269.
27. Behrends, H. W. (1996) Ph.D. Thesis, ETH Zurich, Switzerland.

28. Cremaschi, D., Porta, C., Ghirardelli, R., Manzoni, C., and Caremi, I. (1996) *Biochim. Biophys. Acta 1280*, 27−33.
29. Ashworth, R., Yu, R., Nelson, E. J., Dermer, S., Gershengorn, M. C., and Hinkle, P. M. (1995) *Proc. Natl. Acad. Sci. U.S.A. 92*, 512−516.
30. Enns, C. A., Rutledge, E. A., and Williams, A. M. (1996) in *Biomembranes* (Lee, A. G., Ed.) pp 255−287, JAI Press Inc., Greenwich, Connecticut.
31. Cremaschi, D., Porta, C., and Ghirardelli, R. (1996) *Biochim. Biophys. Acta 1283*, 101−105.
32. Pozvek, G., Hilton, J. M., Quiza, M., Houssami, S., and Sexton, P. M. (1997) *Mol. Pharmacol. 51*, 658−665.
33. Epand, R. M., Stahl, G. L., and Orlowski, R. C. (1986) *Int. J. Pept. Protein Res. 27*, 501−507.
34. Epand, R. M., Epand, R. F., and Orlowski, R. C. (1985) *Int. J. Pept. Protein Res. 25*, 105−111.
35. Arvinte, T., and Drake, A. F. (1993) *J. Biol. Chem. 268*, 6408−6414.
36. Terzi, E., Holzemann, G., and Seelig, J. (1994) *Biochemistry 33*, 7434−7441.
37. Fattal, E., Nir, S., Parente, R. A., and Szoka, F. C. J. (1994) *Biochemistry 33*, 6721−6731.
38. Russell-Jones, G. J., Westwood, S. W., Farnworth, P. G., Findlay, J. K., and Burger, H. G. (1995) *Bioconjugate Chem. 6*, 34−42.

BI981219H